Nanogravimetric and Voltammetric Studies of a Pt-Rh alloy Surface and its Behavior for Methanol Oxidation

R. T. S. Oliveira[1,2], M. C. Santos[3], P. A. P. Nascente[4], L.O.S Bulhões[5], E. C. Pereira[1,*]

[1] Laboratório Interdisciplinar de Eletroquímica e Cerâmica - Centro Multidisciplinar para o Desenvolvimento de Materiais Cerâmicos - Departamento de Química. Universidade Federal de São Carlos – Rodovia Washington Luis, km 235, Caixa Postal 676 CEP – 13565-905 – São Carlos – SP – Brazil
[2] GMEME – Instituto de Química de São Carlos, Universidade de São Paulo, Avenida do Trabalhador San Carlense, 400, Caixa Postal 780, 13566-590, São Carlos, SP, Brazil.
[3] Laboratório de Eletroquímica e Materiais Nanoestruturados – LEMN - Centro de Ciências Naturais e Humanas – CCNH – Universidade Federal do ABC - UFABC – Rua Santa Adélia, 166, Bairro Bangu, CEP 09210-170, Santo André, SP, Brazil.
[4] Departamento de Engenharia de Materiais - Universidade Federal de São Carlos – Rodovia Washington Luis, km 235, Caixa Postal 676 CEP – 13565-905 – São Carlos – SP – Brazil
[5] CENIP, Centro Universitário Central Paulista – UNICEP, Rua Miguel Petroni, 5111 – CEP 13563-470, São Carlos – SP – Brazil.
*E-mail: decp@power.ufscar.br

This paper describes the preparation of a Pt-Rh alloy surface electrodeposited on Pt electrodes and its electrocatalytic characterization for methanol oxidation. The X-ray photoelectronic spectroscopy (XPS) results demonstrate that the surface composition is approximately 24 at-% Rh and 76 % Pt. The cyclic voltammetry (CV) and electrochemical quartz crystal (EQCN) results for the alloy were associated, for platinum, to the well known profile in acidic medium. For Rh, on the alloy, the generation of rhodium hydroxide species ($Rh(OH)_3$ and $RhO(OH)_3$) was measured. During the successive oxidation-reduction cycles the mass returns to its original value, indicating the reversibility of the processes. It was not observed rhodium dissolution during the cycling. The 76 / 24 at % Pt-Rh alloy presented singular electrocatalytic activity for methanol electrooxidation, which started at more negative potentials compared to pure Pt (70 mV). During the sweep towards more negative potentials, there is only weak CO re-adsorption on both Rh and Pt-Rh alloy surfaces, which can be explained by considering the interaction energy between Rh and CO.

Keywords: Pt/Rh alloys, EQCN, XPS, Electrodeposition, methanol electrooxidation.

1. INTRODUCTION

The electrocatalytic oxidation of small organic molecules has been extensively studied due to the interest in the development of fuel-cell anodes [1 - 3]. Several systems have been investigated with the aim of reducing the level of CO poisoning that occurs during the oxidation of methanol, ethanol, formic acid or formaldehyde at Pt-group electrodes [4 - 7].

The study of alloy surfaces is interesting as it is well known that alloying modifies the catalytic properties of transition metals [8] and can also reduce poisoning by CO. Different kinds of alloys have been investigated: Pt-Ru [9], Pt-Sn [10], Pt-Mo [11,12] and Pt-Rh [13]. Among these, several papers report that for Pt-Ru there is a considerable reduction in CO poisoning during methanol oxidation [14,15]. Also, it is widely accepted that Pt-Ru alloys are the most active electrocatalysts for methanol oxidation. But alloying Pt with oxophilic metals, such as Sn and Rh, can also result in a reduction of the methanol oxidation overpotential [15]. Besides, recently [16], Pt-based binary or ternary catalysts containing Rh for use as anodes in direct methanol fuel cells (DMFC) have been synthesized by borohydride reduction method combined with freeze-drying. This proposal shows that the Pt/Rh (2:1) and Pt/Ru/Rh (5:4:1) alloy catalysts showed better catalytic activities for methanol electrooxidation than Pt or Pt/Ru (1:1), respectively. However, the specific role of Rh in alloy catalysts was not evaluated.

The enhancement of the catalytic activity when Pt-Ru alloys are used for methanol electrooxidation is generally related to their superior CO tolerance, as explained by the bifunctional mechanism [17] or by electronic effects [18 – 20]. A mechanism involving a mixture of the two effects has recently been proposed by Waszczuk *et al.* [18].

Many techniques are used for preparing and characterizing electrodeposited films [21 - 23]. Among them, the EQCN technique is an important approach for the investigation of adsorption and electrodeposition processes [24 - 27]. Hence, the simultaneous measurement of the current, charge and the mass changes during alloy electrodeposition, or during the redox processes at a metal or alloy, make the combination of EQCN with cyclic voltammetry a powerful tool to investigate electrochemical processes [21].

In this paper, the electrochemical and spectroscopic characterization of an electrodeposited Pt-Rh alloy using an electrochemical quartz crystal nanobalance (EQCN) coupled with cyclic voltammetry is reported. X-ray photoelectron spectroscopy (XPS) measurements were performed in order to quantify the composition of the Pt-Rh surface. Finally, the electrocatalytic performance of the alloy was evaluated for methanol oxidation using cyclic voltammetry and chronoamperometric techniques.

2. EXPERIMENTAL PART

The working electrode was a Pt film deposited on a 9 MHz AT cut quartz crystal (provided by Seiko EG&G PARC). The platinum electrode was cleaned by oxidation-reduction cycles in 0.1 M HClO$_4$. The geometric area of the Pt electrode was approximately 0.2 cm^2 with a roughness factor of 1.15, as calculated by hydrogen desorption.

The sensitivity factor for the EQCN was determined following the method described previously [28– 30]. The value of the sensitivity factor thus obtained was 800 Hz μg^{-1}. The counter electrode was a Pt foil with a geometric area of 0.5 cm^2. The reference electrode was a hydrogen electrode in the same solution (HESS).

The electroactive areas for Pt [31], Rh [32] and Pt-Rh alloy [33] electrodes were determined by the H-UPD desorption charge. The values obtained for the electroactive areas were used to normalize the cyclic voltammetric and electrochemical quartz crystal microbalance results. The thickness of the catalytic Pt-Rh layer electrodeposited was 40 monolayers, measured by the mass versus time experiment ($\Delta m = 14$ μg cm^{-2} or 3 μg considering the surface area of 0.23 cm^2).

The reagents used were $HClO_4$ (Merck Suprapur®), H_2PtCl_6 (Merck P.A.), and $RhCl_3$ (Merck P.A.). All solutions were prepared with Millipore Milli Q water and purged with oxygen-free nitrogen.

The Pt-Rh alloy was electrodeposited at 0.05 V *vs* HESS for 300 s from a solution of 0.1 M $HClO_4$ that contained 1.7×10^{-4} M H_2PtCl_6 and 3.33×10^{-5} M $RhCl_3$. This alloy was characterized by X-ray photoelectron spectroscopy (XPS) using a Kratos Analytical XSAM HS spectrometer having a Mg Kα (hν= 1253.6 eV) X-ray source, with power supplied by the emission of 15 mA at a voltage of 13 kV. The high-resolution spectra were obtained with an analyzer energy of 20 eV. An Argon ion flux was employed to sputter the surface, with energy of 4 keV, emission of 10 mA and incidence angle of 45°. The samples were analyzed at the electron take-off angle, 90° and 45°, measured with respect to the surface plane. The Shirley background, mixed Gaussian/Lorentzian functions and a least-square routine were used for peak-fitting. The XPS spectrum related to the PtRh alloy was measured after, immediately, removing the sample from the electrochemical cell. However, neither contamination with carbon, oxygen and chlorine atoms nor any evidence of these atoms using cyclic voltammetry and EQCM was observed.

Electrochemical and frequency measurements were carried out at room temperature (25 ^{o}C) using a model 273 EG&G PARC Potenciostat and a model QCA917 Seiko EG&G PARC quartz crystal analyzer, both controlled by an IBM-type PC-486 microcomputer using EG&G PARC M270 software.

3. RESULTS AND DISCUSSION

Figure 1 presents the Pt 4d (1 and 2) and Rh 3d XP-spectra (3 and 4) for the Pt-Rh alloy for the take-off angle of 90°. An overlap of Rh $3d_{3/2}$ and Pt $4d_{5/2}$ occurs at around 312 eV (3). For the binding energy of the Rh 3d doublet (around 950 eV), the escape depth is approximately 6 monolayers for the take-off angle of 90° and approximately 4 monolayers for the take-off angle of 45°. The concentration of Rh was evaluated to be 24 at-%.

The cyclic voltammetric profiles for the Pt electrode (solid line), Rh (2.3 monolayers) electrodeposited on the Pt electrode [34] (dotted line) and Pt-Rh alloy (dashed line) obtained from a 0.1M $HClO_4$ solution are presented in Figure 2a. The behavior of the Pt electrode is described in the literature [30,35]. For the Pt electrode presents typical behavior that corresponds to: i) underpotential deposition and desorption of H at E = 0.05 to 0.4 V, ii) double layer region at E = 0.4 to 0.8 V and iii)

Pt oxide formation in the potential range between 0.8 and 1.55 V. When the potential sweep is reversed, the opposite reactions occur [30,35].
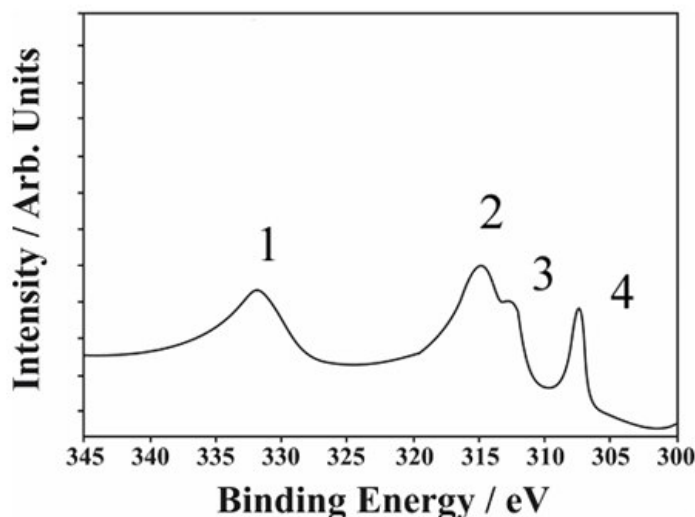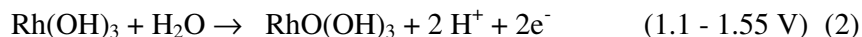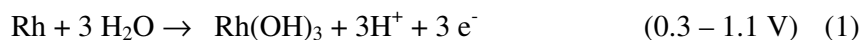

Figure 1. Pt 4d and Rh 3d XPS-spectra for Pt-Rh alloy, acquired at a take-off angle of 90°.

The corresponding mass response for the Pt electrode is presented in Figure 2b. During the positive potential sweep, the following reactions occur: a) H UPD desorption and water incorporation on the electrode surface (between 0.05 and 0.4 V, $\Delta m = 40$ ng cm^{-2}), b) adsorption of anions ($ClO_4^-.2$ H_2O) between 0.4 V and 1 V ($\Delta m = 20$ ng cm^{-2}) and c) Pt oxide formation (0.8 and 1.55 V, $\Delta m = 40$ ng cm^{-2}). During the negative potential sweep (1.55 to 0.05 V), reduction of Pt oxide, desorption of anions and water and H adsorption occur, leaving the surface with the original mass value [30,36,37].

For the Rh electrode (electrodeposited on a Pt substrate), the cyclic voltammetric profile presented in Figure 2a can be described by: i) hydrogen adsorption on the Rh layer (0.05 to 0.3 V), ii) Rh oxidation (0.3 to 1.1 V) and the formation of $Rh(OH)_3$ ($\Delta m = 100$ ng cm^{-2}) and iii) $Rh(OH)_3$ oxidation to $RhO(OH)_3$ ($\Delta m = 40$ ng cm^{-2}). Sweeping the potentials towards more negative values, total Rh oxide reduction and H adsorption on Rh occur. The formation of rhodium oxide species was recently described by Oliveira et al. [34] as:

$$Rh + 3\ H_2O \rightarrow\ Rh(OH)_3 + 3H^+ + 3\ e^- \qquad (0.3 - 1.1\ V) \quad (1)$$
$$Rh(OH)_3 + H_2O \rightarrow\ RhO(OH)_3 + 2\ H^+ + 2e^- \qquad (1.1 - 1.55\ V) \quad (2)$$

The results obtained here are in agreement with this mechanism.

The voltammetric behavior of the Pt-Rh alloy (24 at-% Rh) is presented in Figure 2a. A mixed profile that involves both Pt and Rh can be observed, as expected for Pt-Rh alloys [38]. However, Rh dissolution was not observed in the results obtained here, contrary to those described for Pt-Rh in H_2SO_4 solutions [38,39].

The mass profile for the Pt-Rh alloy (Figure 2b) can be described as: i) formation of rhodium hydroxide ($Rh(OH)_3$ between 0.35 and 1.1 V (reaction 1), ii) formation of PtO and $RhO(OH)_3$ between 1.1 and 1.55 V. During the reverse sweep the oxide reduction process occurs at different potentials: for PtO at 0.7 V and $RhO(OH)_3$ between 0.5 V and 0.05 V. A secondary reaction (H adsorption) was also expected in the same region as rhodium oxide reduction, as described for Rh electrodeposited on Pt [34]. Using surface composition obtained by XPS (24 at-% of Rh and 76 at-% of Pt), the nanogravimetric data (see Figure 2b) can be ascribed to: i) hydrogen desorption from Pt (coverage of 76 at-%) with simultaneous water adsorption (31 ng cm^{-2}) between 0.05 and 0.35 V, ii) rhodium oxide formation ($Rh(OH)_3$) (coverage of 24 at-%, $\Delta m = 25$ ng cm^{-2}), anion adsorption on Pt (coverage of 7 at-% – $ClO_4.2\ H_2O$, $\Delta m = 19$ ng cm^{-2}), platinum oxide formation (coverage of 76 at-%, $\Delta m = 31$ ng cm^{-2}) and rhodium oxide formation $RhO(OH)_3$ (coverage of 24 at-%, 10 ng cm^{-2}). The overall mass variation between 0.35 V and 1.55 V was 85 ng cm^{-2}, which is close to the experimentally obtained value (90 ng cm^{-2}).
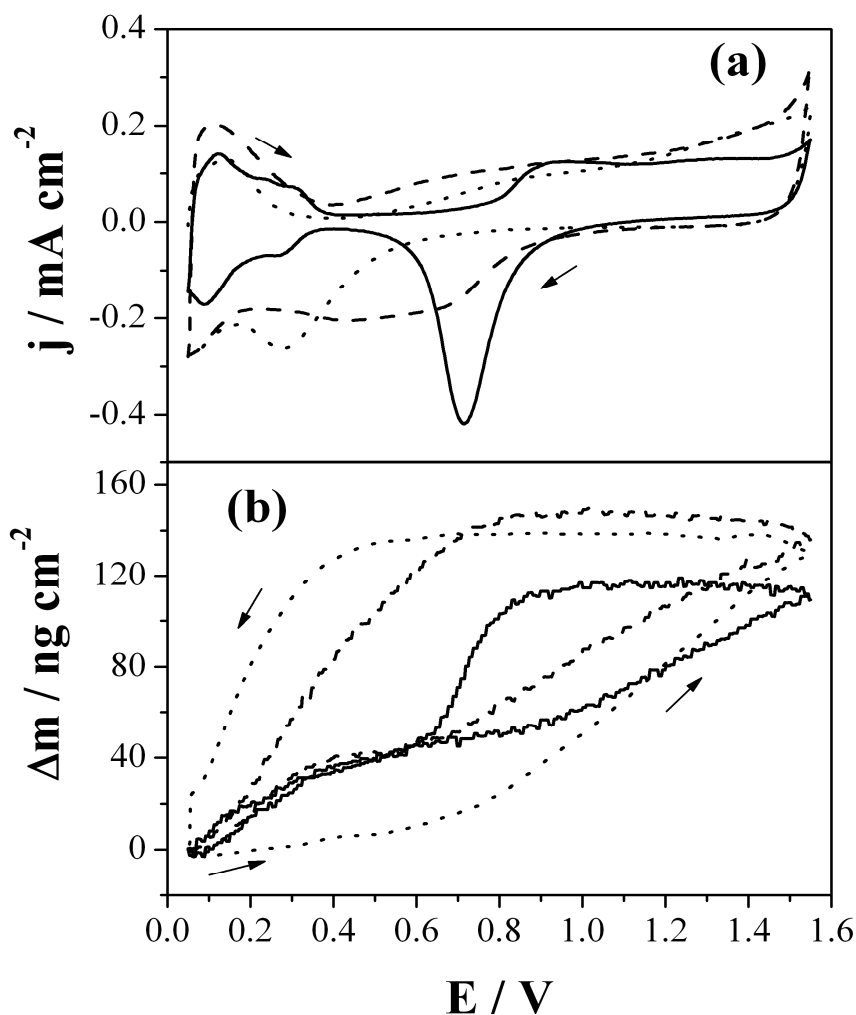

Figure 2. (a) Voltammetric profile of: Pt (solid line), Rh (dotted line) and Pt/Rh alloy (24% Rh, dashed line). (b) Mass profile of: Pt (solid line), Rh (dotted line) and Pt/Rh alloy (24% Rh, dashed line). The electrolyte was 0.1 M $HClO_4$ and the sweep rate = 0.1 V s^{-1}.

Comparing Figures 2a and 2b, it becomes clear that the oxidation of the surface that contains 24 at-% Rh begins at 0.3 V (represented by the current and mass increases), which is more negative than that observed for the pure Pt surface (0.8 V). It can be proposed that the enhanced behavior for methanol oxidation at the Pt-Rh alloy (compared to Pt) could be due to the generation of rhodium oxide species $(Rh(OH)_x)$ at these low potentials.
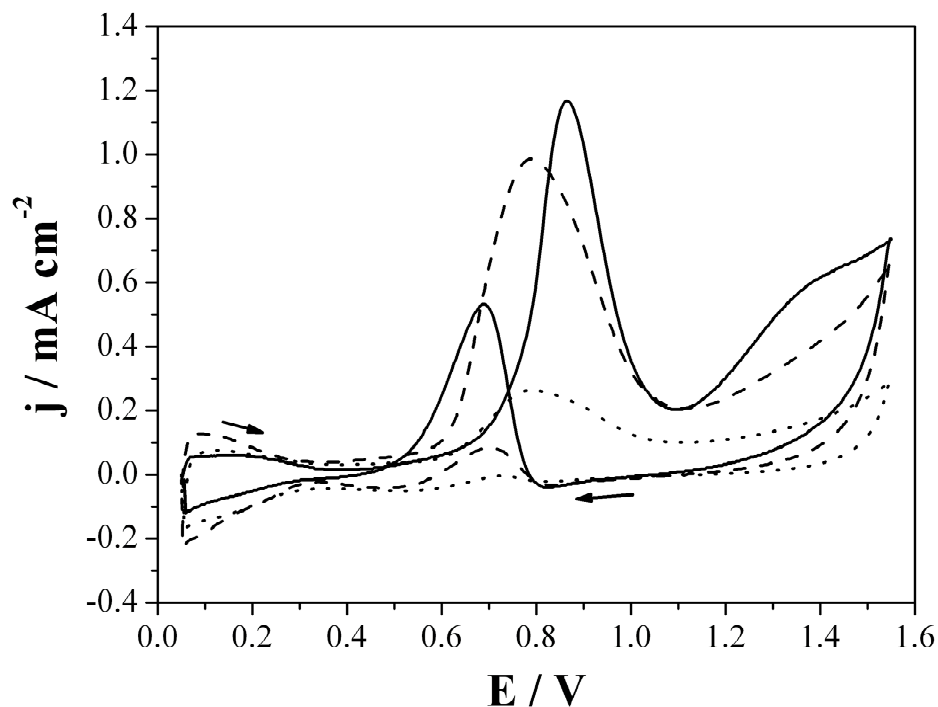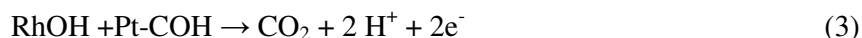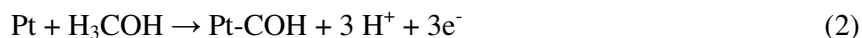

Figure 3. Voltammetric profile of methanol oxidation (0.5 M) in 0.1 M $HClO_4$ at polycrystalline Pt (solid line), at Rh (dotted line) and at Pt/Rh alloy (24% Rh, dashed line). Sweep rate = 0.1 V s^{-1}.

In Figure 3 methanol oxidation was investigated over three substrates: Pt (solid line), 2.3 monolayers of Rh (dotted line) and Pt-Rh alloy with 24 at-% of rhodium (dashed line). In the presence of methanol Pt presents the well-known oxidation profile [40,41] characterized by two oxidation peaks at 0.85 V and 1.25 V during the positive sweep. The first process is attributed to the oxidative removal of adsorbed/dehydrogenated methanol fragments (CO_{ads} for example) by oxygen-containing species PtOH [42,43]. During this process, which occurs at 0.85 V, CO, CO_2, HCOOH, HCOH, and $HCOOCH_3$ are formed and CO molecules are re-adsorbed, poisoning the surface [40,44]. The second anodic process (current peak at 1.25 V) can be attributed to the oxidation of the species produced [45,46]. During the sweep toward negative potentials from 1.55 V to 0.05 V, the Pt oxide is reduced. This process reactivates the surface and the methanol oxidation reaction occurs as indicated by the presence of an intense anodic peak in the double-layer region at 0.69V. Fig. 3 (dotted line) presents the behavior of 2.3 monolayers of Rh electrodeposited on Pt, which displayed poor catalytic activity for methanol electrooxidation in the positive sweep. As it has been proposed recently [47] using both electrochemical and surface-enhanced raman spectroscopic studies show Rh has no discernible activity

toward the electrooxidation or dissociation of methanol in acidic solutions. Rh becomes active and its activity increases with the decrease of the solution acidity. Besides, it has been discussed using first principles quantum mechanics [non-local density functional theory (B3LYP)] [48] that the overall methanol oxidation reaction can be considered in three stages in transition metals (Pt, Ir, Os, Pd, Rh, and Ru): (1) dehydrogenation of methanol, (2) dehydrogenation of water, and (3) formation of the second C-O bond. For pure Pt, it has been found that $(CO)_{ads}$ is the thermodynamic sink in the reaction, in agreement with experimental evidence that this species poisons catalytic activity if not actively removed from the surface. In the six metals including rhodium, methanol dehydrogenation is most facile on Pt. For water dehydrogenation, Ru is the most active while Pt performs very poorly. These results support the bifunctional mechanism of Pt-Ru or Pt-Rh whereby Pt is responsible for the dehydrogenation of methanol and Rh or Ru for the dehydrogenation of water.

During the potential sweep toward negative potentials from 1.55 to 0.05 V the behavior observed (a low current for methanol oxidation) is suggested to be explained by weak CO re-adsorption on the electrode surface. Van Santen [49] observed the weak interaction between CO and Rh. Furthermore, the high energy for CO adsorption on Rh [50], as compared to Pt, can probably explain the low currents observed for methanol oxidation on Rh. Furthermore, methanol dehydrogenation is easier on Pt compared with rhodium [48].

Methanol electrooxidation at the Pt-Rh alloy is presented in Figure 3 (dashed line). In agreement with literature data, the best Pt-Rh alloy composition for methanol electrooxidation is of about 20-30% at % in Rh where there is a synergistic effect which causes the highest activity [38,39]. Furthermore, the catalytic activity of Pt-Rh alloys for oxidation of pure-hydrogen or CO-contaminated hydrogen exhibited a maximum at 24 % Rh [33]. For these reasons, it was decided to use the composition 24% at % in Rh. Methanol oxidation on a Pt electrode starts at 0.42 V vs. HESS. At the alloy, electrooxidation begins 70 mV more negative than for the Pt electrode. The anodic peak potential for methanol oxidation at the Pt-Rh alloy was also observed to be more negative (0.79 V) than at Pt (0.87 V). In the reverse sweep the alloy displayed a significant decrease in the CO re-adsorption process and the current density peak is at 0.7 V vs. HESS. The decrease in the re-adsorption process it is suggested to be explained by the repulsive interaction of CO with hydroxide species that are present in the alloy [49] Thus, the voltammetric results for methanol oxidation on the Pt-Rh alloy showed an enhanced activity when compared to Pt. In fact, this behavior can probably be explained by considering the generation of oxygenated Rh species (Rh(OH)) at more negative potentials when compared to Pt, as described for Figures 2a and 2b, and this effect could be associated with the bifunctional mechanism that has been discussed for other binary systems [17,40]:

$$Rh + H_2O \rightarrow RhOH + H^+ + e^- \qquad (1)$$
$$Pt + H_3COH \rightarrow Pt\text{-}COH + 3\ H^+ + 3e^- \qquad (2)$$
$$RhOH + Pt\text{-}COH \rightarrow CO_2 + 2\ H^+ + 2e^- \qquad (3)$$

As suggested for Ru [18], another important factor could involve a change in the electron density of Pt, which leads to the weakening of the CO-Pt bond, or a mixture of both effects.

The chronoamperometric experiments performed at 0.5 V vs. HESS (Figure 4) demonstrated that the Pt-Rh alloy (dashed line) presented higher electrocatalytic activity compared to Pt (solid line). It can be observed that the oxidation current for methanol (0.5M) in $HClO_4$ at Pt decreases rapidly compared to the Pt-Rh alloy, due to irreversible CO poisoning. The Pt-Rh alloy studied here presents higher activity for methanol oxidation than pure Pt (the current during constant polarization is about 280 % higher for Pt-Rh compared to Pt). The current increase is due to a reduced amount of CO adsorption. This reduction is the result of the generation of oxy-hydroxyl species at more negative potentials when Rh is present (24 at-%) than for pure Pt. These rhodium hydroxide species react with the CO adsorbed on Pt and liberate sites for methanol oxidation.
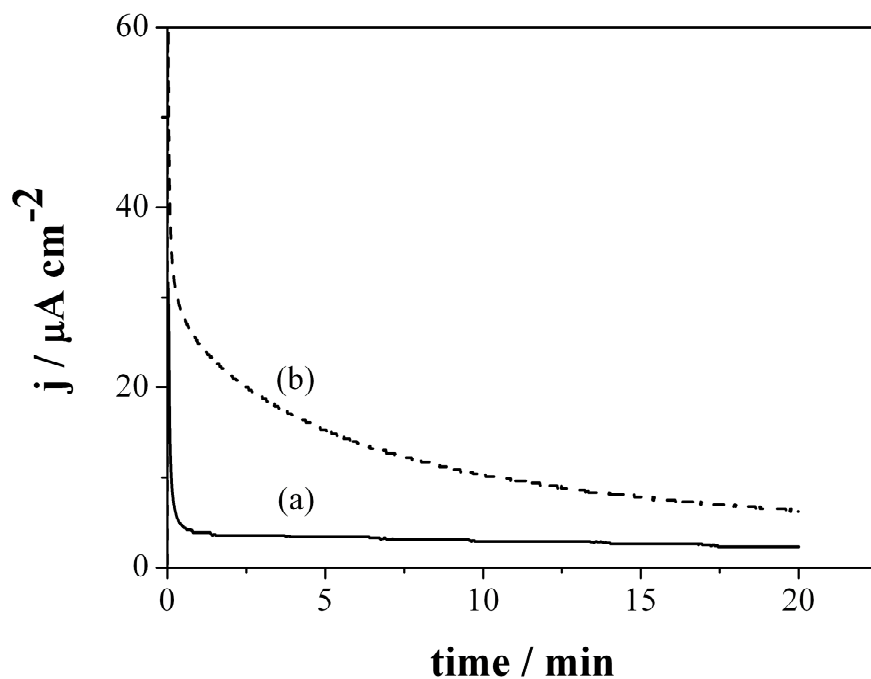

Figure 4. Chronoamperometric measurements of methanol oxidation at (a) Pt (solid line) and (b) Pt-Rh alloy (24% Rh, dashed line). E_{ox} = 0.5 V and t = 20 min. $[H_3COH]$ = 0.5 M in 0.1 M $HClO_4$.

Although, the results for methanol oxidation over the Pt-Rh showed as enhancement of the eletrocatalytical performance when compared to platinum, the Pt-Ru alloy [51] showed a higher catalytic activity than that one here measured. However, the catalytic activity depends on the ratio of Pt, Ru or Rh in the alloy. Recently [16], it was pointed out that Pt/Rh (2:1) and Pt/Ru/Rh (5:4:1) alloy catalysts showed better catalytic activities for methanol electrooxidation than Pt or Pt/Ru (1:1), respectively. Then, considerable effort continues to be focused on the developed of a new ternary or quaternary alloy catalysts [16,52]. These alloys will be a theme of our further work.

4. CONCLUSIONS

In this paper the XPS, EQCN and voltammetric characterization of Pt-Rh alloy surface has been described. The effect of this alloy surface on methanol oxidation was also investigated. XPS

experiments indicate the formation of a Pt-Rh alloy with a composition of 24 at-% Rh and 76 at-% Pt. The EQCN and cyclic voltammetric measurements indicated that the mass and current profiles can be ascribed as: i) the oxidation of rhodium with the formation of $Rh(OH)_3$ and $RhO(OH)_3$ (24 at-%) and ii) the processes of hydrogen adsorption/desorption on Pt, Pt oxide formation and reduction (PtO) and anion adsorption ($ClO_4^-2H_2O$) (taking into account 76 at-% of exposed platinum).

The electrocatalytical activity of the Pt-Rh alloy surface is improved because the electrooxidation potential of methanol is 70 mV more negative than for Pt. The density current for methanol oxidation over the Pt-Rh alloy is also higher than on Pt before 0.8 V. In addition, during the reverse sweep there is only weak CO re-adsorption, which is associated with the weak interaction of CO with Rh, the high energy of CO adsorption on Rh and the repulsive interaction between rhodium hydroxide and CO.

Chronoamperometric measurements for methanol oxidation presented a current increase of approximately 280 % for the Pt-Rh alloy compared with pure platinum during constant polarization (0.5 V) for 20 minutes. This observation indicates that there is a reduction in the poisoning effect of strongly adsorbed CO molecules, which is related to the presence of rhodium in the alloy and the generation of oxy-hydroxyl species at more negative potentials than for Pt.

References

1. B. Beden, C. Lamy, J.-M. Leger, In Modern Aspects of Electrochemistry, J. O. Bockris, B. E. Conway, R. E. White, Eds., Plenum, New York, 1992, Vol. 22.
2. R. Parsons, T. Vandernoot, *J. Electroanal. Chem.*, 257 (1988) 9.
3. T. Iwasita, W. Vielstich, In Advances in Electrochemical Sciences and Engineering; H. Gerischer, C. W. Tobias, Eds., VCH, Weinheim, 1990; Vol. 1.
4. J. Jiang, A. Kucernak, *J. Electroanal. Chem.*, 543 (2003) 187.
5. E. I. Santiago, G. A. Camara, E. A. Ticianelli, *Electrochim. Acta*, 48 (2003) 3527.
6. T. Kawaguchi, W. Sugimoto, Y. Murakami, Y. Takasu, *Electrochem. Commun.,* 6 (2004) 480.
7. E. V. Spinacé, A. O. Neto, M. Linardi, *J. Power Sources*, 129 (2004) 121.
8. Q. Ge, S. Desai, M. Neurock, K. Kourtakis, *J. Phys. Chem. B,* 105 (2001) 9533.
9. L. Dubau, F. Hahn, C. Coutanceau, J.-M. Leger, C. Lamy, *J. Electroanal. Chem.*, 554-555 (2003) 407.
10. C. Panja, N. Saliba, B. E. Koel, *Surf. Sci.*, 395 (1998) 248.
11. H.F. Oetjen, V.M. Schmidt, U. Stimming, F. Trila, *J. Electrochem. Soc.*, 143 (1996) 3838.
12. A. Gasteiger, N. Markovic, P.N. Ross, E.J. Cairns, *J. Phys. Chem.*, 98 (1994) 617.
13. J. P. I. de Souza, S. L. Queiroz, K. Bergamaski, E. R. Gonzalez, F. C. Nart, *J. Phys. Chem. B*, 106 (2002) 9825.
14. S. Wasmus, A. Kuver, *J. Electroanal. Chem.*, 461 (1999) 14.
15. B. Gurau, R. Viswanathan, R. Liu, T. J. Lafrenz, K. L. Ley, E. S. Smotkin, E. Reddington, A. Sapienza, B. C. Chan, T. E. Mallouk, S. Sarangapani, *J. Phys. Chem. B*, 102 (1998) 9997.
16. Jong-Ho Choi, Kyung-Won Park, In-Su Park, Woo-Hyun Nam, Yung-Eun Sung*., Electrochim. Acta*, 50 (2004) 787.

17. M. Watanabe, S. Motoo, *J. Electroanal. Chem.*, 60 (1975) 267.
18. P. Waszczuk, A. Wieckowski, P. Zelenay, S. Gottesfeld, C. Coutanceau, J.-M. Leger, C. Lamy, *J. Electroanal. Chem.*, 511 (2001) 55.
19. P. Waszczuk, G.U. Lu, A. Wieckowski, C. Lu, C. Rice, M.I. Masel, *Electrochim. Acta*, 47 (2002) 36.
20. C. Lu, C. Rice, M.I. Masel, P.K. Babu, P. Waszczuk, H.S. Kim, E. Oldfield, A. Wieckowski, *J. Phys. Chem. B*, 106 (2002) 9581.
21. L. S. Sanches, S. H. Domingues, C. E. B. Marino, L. H. Mascaro, *Electrochem. Commun.*, 6 (2004) 543.
22. A. Grigucevicien, K. Leinartas, R. Juskenas, E. Juzeliunas, *J. Electroanal. Chem.*, 565 (2004) 203.
23. T. Aokia, Y. Changb, G. Badanob, J. Zhaob, C. Greinb, S. Sivananthanb, D.J. Smitha, *J. Crys. Growth*, 265 (2004) 224.
24. A. Wieckowski, Interfacial Electrochemistry, Theory, Experiment and Applications, Marcel Dekker, Inc., New York – Basel, 1999, p. 570.
25. M. Zhou, N. Myung, X. Chen, K. Rajeshwar, *J. Electroanal. Chem.*, 398 (1995) 5.
26. D. Hamm, C.-O.A. Olsson, D. Landolt, *Corrosion Science*, 44 (2002) 1009.
27. H. Uchida, H. Ozuka, M. Watanabe, *Electrochim. Acta*, 47 (2002) 3629.
28. S. Bruckenstein, S. Swathirajan, *Electrochim. Acta*, 30 (1985) 851.
29. B. Keita, L. Nadjo, D. Belanger, C.P. Wilde, M. Hilaire, *J. Electroanal. Chem.*, 384 (1995) 155.
30. M.C. Santos, D.W. Miwa, S.A.S. Machado, *Electrochem. Commun.*, 2 (2000) 692.
31. S. Trasati, O. A. Petri, *Pure and Appl. Chem.*, 63 (1991) 719.
32. R. Woods, *J. Electroanal. Chem.*, 49 (1974) 217.
33. P. N. Ross, K. Kinoshita, A. J. Scaperllino, P. Stonehart, *J. Electroanal. Chem.*, 59 (1975) 177.
34. R. T. S. Oliveira, M. C. Santos, L. O. S. Bulhões, *J. Eletroanal. Chem.*, 569 (2004) 233.
35. B. E. Conway, Progress in Surface Science, 49 (1995) 331.
36. H. Uchida, N. Ikeda, M. Watanabe, *J. Electroanal. Chem.*, 424 (1997) 5.
37. H. Uchida, M. Hiei, M. Watanabe, *J. Electroanal. Chem.*, 425 (1998) 97.
38. N.R. Taconi, J.M. Leger, B. Beden, C. Lamy, *J. Eletroanal. Chem.*, 134 (1982) 117.
39. D.F. Koch, D. A. J. Rand, R. Woods, *J. Eletroanal. Chem.*, 70 (1976) 73.
40. T. Iwasita, *Electrochim. Acta*, 47 (2002) 3663.
41. F. Kadirgan, B. Beden, J. M. Leger, C. Lamy, *J. Electroanal. Chem.*, 127 (1981) 75.
42. H. A. Gasteiger, N. Markovic, P. N. Ross, E. J. Cairns, *J. Electrochem. Soc.*, 141 (1994) 1795.
43. T. Zerihun, P. Grundler, *J. Electroanal. Chem.*, 441 (1998) 57.
44. L. -W. H. Leung, M. J. Weaver, *J. Phys. Chem.*, 92 (1988) 4019.
45. L. -W. H. Leung, M. J. Weaver, *Langmuir*, 6 (1990) 323.
46. Y. Xu, A. Armini, M. Schell, *J. Electroanal. Chem.*, 398 (1995) 95.
47. Xu-Feng Lin, Bin Ren, Zhong-Qun Tian, *J. Phys. Chem. B* , 108, (2004) 981.
48. Jeremy Kua, W. A. Goddard III, *J. Am. Chem. Soc.*, 121 (1999) 10928.
49. R. A. Van Santen, A. de Koster, T. Koerts, *Catal. Lett.*, 7 (1990) 1.
50. M. P. Aum Mallen, L. D. Schmidt, *J. Catal.*, 161 (1996) 230.
51. E.A. Batista, H. Hoster, T. Iwasita, *J. Electroanal. Chem.*, 554-/555 (2003) 265.
52. Kyung-Won Park, Jong-Ho Choi, Seol-Ah Lee, Chanho Pak, Hyuck Chang, Yung-Eun Sung, *J. Catal.*, 224 (2004) 236.